

# Stereochemical Rigidity in $ML_5$ Complexes. III. Detailed Line Shape Analysis and Rearrangement Barriers in Pentakisphosphite Complexes of Cobalt(I), Rhodium(I), Iridium(I), Nickel(II), Palladium(II), and Platinum(II)

J. P. Jesson\* and P. Meakin

Contribution No. 2076 from the Central Research Department,  
E. I. du Pont de Nemours & Company, Experimental Station,  
Wilmington, Delaware 19898. Received December 8, 1973

**Abstract:** An nmr investigation has been carried out for a class of cationic  $ML_5$  complexes ( $M = Co, Rh, Ir, Ni, Pd,$  and  $Pt,$  and  $L =$  phosphite). More than 20 complexes were studied, all of which are stereochemically nonrigid at ambient temperatures and stereochemically rigid on the nmr time scale at low temperatures. The rearrangements are shown to be intramolecular by observation of retention of metal-phosphorus coupling in the high temperature limit for the  $A_2B_3X$  spin systems and by observing the invariance of the spectra to excess ligand for the  $A_2B_3$  spin systems. A series of complete density matrix calculations for intramolecular exchange have been carried out, and the permutational nature of the exchange has been established for specific complexes of  $Pd(II), Ni(II), Co(I),$  and  $Rh(I)$ ; in all cases the rearrangements involve simultaneous exchange of the axial ligands with a pair of equatorial ligands in the trigonal bipyramidal ground state structure and are therefore consistent with the Berry process. Barriers lie within the range 5–12 kcal mol<sup>-1</sup> and increase with increasing steric bulk of the phosphite ligand up to the point where the bulk is too great for  $ML_5$  complexes to be formed (*i.e.*, where the ligand dissociation equilibrium  $ML_5 \rightleftharpoons ML_4 + L$  lies well to the right). For a given ligand, barriers are relatively insensitive to variation of the central metal although the ordering  $Co > Ir \simeq Ni > Rh > Pt > Pd$  can be established; thus sequences  $Co > Rh < Ir$  and  $Ni > Pd < Pt$  apply and the members of the first triad have uniformly higher barriers than those of the corresponding members of the second triad.

In earlier papers in this series, we have presented the first evidence for the stereochemical rigidity of  $ML_5$  species in solution.<sup>1–4</sup> In the present paper, we describe an nmr study of the intramolecular exchange processes in  $ML_5$  cations for the six metals ( $Co, Rh, Ir, Ni, Pd, Pt$ ). At low temperatures they all show  $A_2B_3$  or  $A_2B_3X$   $^3P\{^1H\}$  nmr patterns. As the temperature is raised, the spectra broaden and coalesce into a single line ( $A_5$  spectrum) or a doublet ( $A$  part of  $A_5X$  spectrum). Maintenance of  $A-X$  coupling ( $A_5X$  cases) and invariance to added ligand ( $A_5$  cases) show that the rearrangements are intramolecular. The variation of chemical shift with temperature noted in some species<sup>1,2</sup> and thought possibly to arise from ion pairing effects is found not to be a general feature of the spectra of these complexes. Concentration, solvent, and anion variation studies eliminate ion pairing as an important factor in the dynamic behavior of the cations.

Activation parameters for rearrangements have been determined for the majority of the complexes and mechanistic studies have been carried out for  $Co[P(OCH_2)_3CCH_3]_5^+$  and  $Ni[P(OCH_2)_3CC_2H_5]_5^{2+}$  using a complete density matrix treatment; the results show the same basic permutational behavior established for  $Rh[P(OCH_3)_3]_5^+$  earlier<sup>2</sup> and exclude any physical mechanisms which involve single axial-equatorial exchanges. They are consistent with the Berry process<sup>5</sup> as well as some other proposed mechanisms such as the turnstile rotation.<sup>6</sup>

The barriers to rearrangement range from 6 to 12 kcal mol<sup>-1</sup> and increase with increasing ligand steric bulk for a given metal; the relationships  $Co > Rh < Ir$  and  $Ni > Pd < Pt$  are established for variation of the central metal for a given ligand, with the members of the cobalt triad having uniformly higher barriers than the corresponding members of the nickel triad.

## Experimental Section

The preparation and initial studies of the intermolecular exchange behavior of the complexes investigated in this study have been described.<sup>4</sup> In a number of cases it proved convenient to prepare complexes *in situ* in nmr tubes.

The  $^3P\{^1H\}$  and  $^{13}C\{^1H\}$  nmr spectra were obtained using a Bruker HFX 90-Digilab FTS/NMR-3 system as previously described.<sup>2</sup>

The line shape calculations use density matrix methods<sup>7,8</sup> coupled with group theoretical methods of permutational analysis and computer techniques for symmetry factoring.<sup>2,9,10</sup>

## Results

Low temperature limit nmr spectral parameters for all compounds considered in this section are given in the preceding publication.<sup>4</sup>

**A. Rhodium.** The low temperature limit spectra are  $A_2B_3X$  patterns showing that the complexes have  $D_{3h}$  symmetry (configuration 1) on the nmr time scale.<sup>2,4</sup> Detailed analyses of the temperature dependence of the  $^3P\{^1H\}$  spectra for a range of  $RhL_5^+$  complexes have been presented earlier. Data for one

(1) J. P. Jesson and P. Meakin, *J. Amer. Chem. Soc.*, **95**, 1344 (1973).

(2) Paper I in this series: P. Meakin and J. P. Jesson, *J. Amer. Chem. Soc.*, **95**, 7272 (1973).

(3) J. P. Jesson and P. Meakin, *J. Inorg. Nucl. Chem. Lett.*, **9**, 1221 (1973).

(4) Paper II in this series: P. Meakin and J. P. Jesson, *J. Amer. Chem. Soc.*, **96**, 5751 (1974).

(5) R. S. Berry, *J. Chem. Phys.*, **32**, 933 (1960).

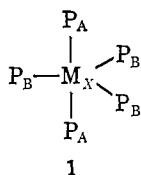
(6) I. Ugi, D. Marguarding, H. Klusacek, P. Gillespie, and F. Ramirez, *Accounts Chem. Res.*, **4**, 288 (1971).

(7) J. I. Kaplan, *J. Chem. Phys.*, **28**, 278 (1958); **29**, 462 (1958).

(8) S. Alexander, *J. Chem. Phys.*, **37**, 967, 974 (1962); **38**, 1787 (1963); **40**, 2741 (1964).

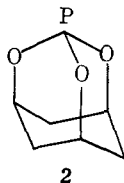
(9) P. Meakin, E. L. Muettterties, F. N. Tebbe, and P. J. Jesson, *J. Amer. Chem. Soc.*, **93**, 4701 (1971).

(10) J. P. Jesson and P. Meakin, *Accounts Chem. Res.*, **6**, 269 (1973).



additional  $RhL_5^+$  compound have been obtained since the original publication and these are described below.

(i)  $Rh(\text{phosphoradamantane})_5^+B(C_6H_5)_4^-$ . This complex (phosphoradamantane = 2,8,9-trioxaphosphaadamantane (configuration 2)) was prepared *in situ*



in the nmr tube.<sup>4</sup> The temperature dependence of the chemical shift separation is quite small but larger than for complexes with the more rigid sterically less bulky ligands of the type  $P(OCH_2)_3CR$ . For  $Rh(\text{phosphoradamantane})_5^+B(C_6H_5)_4^-$  the spin system is more tightly coupled ( $|J_{AB}|/|\delta_A - \delta_B|$  is larger) than for other  $RhL_5^+$  cations which we have investigated<sup>2</sup> giving rise to a less easily recognized  $A_2B_3X$  spectrum.<sup>4</sup>

From an nmr line shape analysis a rate of  $75 \text{ sec}^{-1}$  is obtained at  $-64^\circ$  corresponding to a free energy of activation of  $10.25 \text{ kcal mol}^{-1}$  at this temperature. An exchange process involving simultaneous exchange of the two axial ligands with two of the equatorial ligands was assumed.

**B. Cobalt.** (i)  $Co[P(OC_2H_5)_3]_5^+Cl^-$ .<sup>11</sup> The temperature dependence of  $^{31}P\{^1H\}$  nmr spectra of  $Co[P(OC_2H_5)_3]_5^+Cl^-$  in  $CHClF_2$  solution is shown in Figure 1, together with a set of calculated spectra. The calculated spectra were obtained using an  $A_2B_3$  model in which the only parameter varied was the chemical shift separation between the A and B nuclei. It can be seen that the calculations give excellent agreement with the experimental data. Superficially the observed temperature-dependent spectra appear to correspond to a classical line shape variation normally associated with chemical exchange (broadening of a sharp, complex, low temperature spectrum with increasing temperature and finally, at higher temperatures, collapse into a single line) but the simulation is obtained *without assuming exchange*. This is a fortuitous case in which the chemical shift variation with temperature is large and the magnitude of the shift goes from an easily measurable value to a very small value over the temperature range studied. The example indicates the danger of assuming the presence of an exchange process on the basis of qualitative line shape effects; the good agreement with calculation indicates that the cation has  $D_{3h}$  symmetry on the nmr time scale over essentially the whole temperature range shown in Figure 1. Exchange almost certainly occurs when the temperature is raised still further (it would be difficult to detect with the almost zero chemical shift separation) but there is *no clear evidence for exchange* on the basis of the data in Figure 1. In obtaining the calculated spectra the AB

(11) We are indebted to Dr. L. W. Gosser for a sample of this complex.

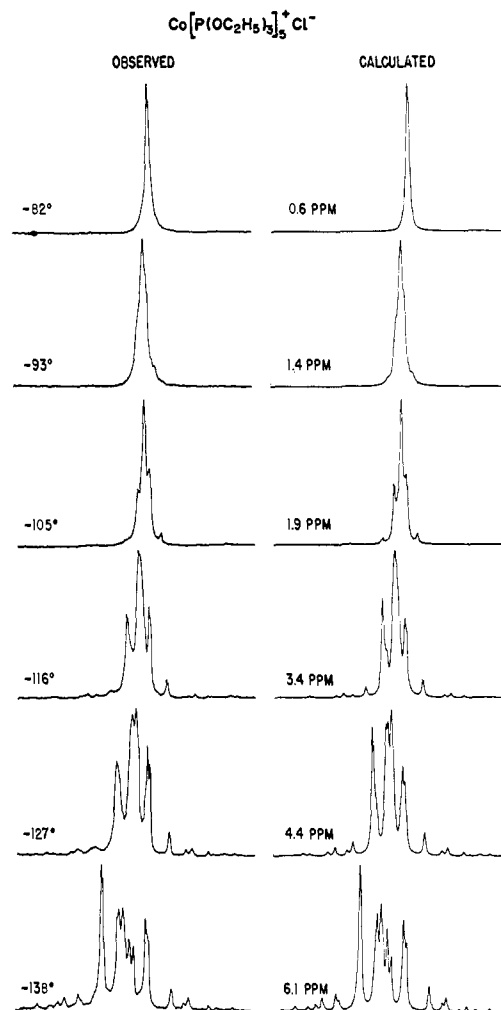


**Figure 1.** The temperature-dependent Fourier mode  $^{31}P\{^1H\}$  nmr spectra for a solution of  $Co[P(OC_2H_5)_3]_5^+Cl^-$  in  $CHClF_2$ . The only parameter varied to obtain the corresponding calculated spectra was the chemical shift difference between the axial and equatorial phosphorus sites. This chemical shift separation is given with the simulated spectra.

coupling constant was kept fixed at 148 Hz (the value obtained by fitting the  $-138^\circ$  spectrum) and the AB chemical shift separation was varied to give a good fit to the observed spectra. A case similar to the one discussed above, where qualitatively there is ambiguity as to whether chemical shift variation or exchange behavior accounts for the spectral variation with temperature, is discussed in the section dealing with iridium complexes; for the iridium species  $Ir[P(OCH_2)_3CCH_3]_5^+$  the calculations show that in this case *exchange processes* account for the line shape behavior.

Before considering other cobalt complexes, one additional feature in Figure 1 deserves mention; in the lower temperature range there is some disagreement between the observed and calculated spectra. This arises because in the experimental spectrum the lines largely associated with the equatorial phosphorus nuclei (low field section of spectrum) are broader than those largely associated with the axial phosphorus nuclei. Effects of this type were observed only for the  $CoL_5^+$  complexes and are attributed to partial decoupling of the  $^{31}P-^{59}Co$  spin-spin coupling resulting from the rapid quadrupole relaxation of the  $^{59}Co$  nucleus with spin  $I = 7/2$ . At low temperature ( $-138^\circ$ ) the quadrupole relaxation is

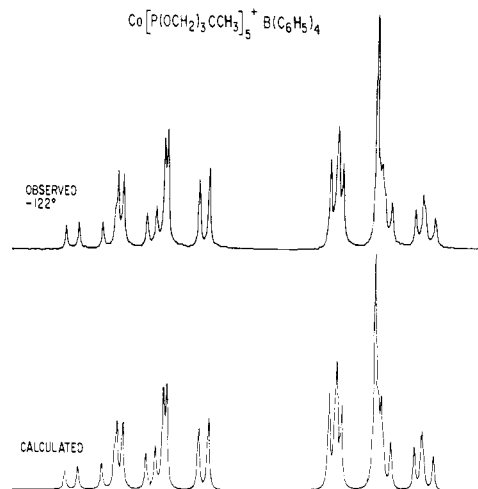


**Figure 2.** Low temperature limit Fourier mode  $^{31}\text{P}\{^1\text{H}\}$  nmr spectrum for a solution of  $\text{Co}[\text{P}(\text{OCH}_2)_3\text{CCH}_3]_5^+ \text{B}(\text{C}_6\text{H}_5)_4^-$  in chlorodifluoromethane. The calculated spectrum was obtained using an  $\text{A}_2\text{B}_3$  model.

very effective (the rotational correlation times are long because of the relatively high viscosity and low temperature); as a result, the decoupling is almost complete and the line width variations across the spectrum are small. As the temperature is raised the line shape effects due to quadrupole relaxation become more pronounced. The lines to low field are broader because  $J_{\text{PnCo}} > J_{\text{PaCo}}$  (configuration 1). Above the temperature range shown in Figure 1, the spectrum broadens again as the viscosity of the solution decreases and the quadrupole decoupling of the  $^{31}\text{P}$ - $^{59}\text{Co}$  spin-spin coupling becomes less effective.

(ii)  $\text{Co}[\text{P}(\text{OCH}_2)_3]_5^+ \text{B}(\text{C}_6\text{H}_5)_4^-$ . The temperature-dependent  $^{31}\text{P}\{^1\text{H}\}$  nmr spectra of this complex in chlorodifluoromethane over the temperature range  $-140$  to  $-70^\circ$  are very similar to those shown in Figure 1 except that now the chemical shift associated with the equatorial phosphorus nuclei is upfield.

The  $^{31}\text{P}\{^1\text{H}\}$  spectrum at  $-138^\circ$  is almost a mirror image of the low temperature limit spectrum for  $\text{Co}[\text{P}(\text{OC}_2\text{H}_5)_3]_5^+$  (Figure 1). Again, the chemical shift difference decreases in magnitude as the temperature is increased and the spectrum coalesces into a single line; there is no evidence for an intramolecular exchange process in these spectra. The lines to the upfield side of the spectrum are broader than those to the downfield side indicating (see section B (i)) that, as for  $\text{Co}[\text{P}(\text{OC}_2\text{H}_5)_3]_5^+$ ,  $J_{\text{PnCo}} > J_{\text{PaCo}}$  (configuration 1).

(iii)  $\text{Co}[\text{P}(\text{OCH}_2)_3\text{CCH}_3]_5^+ \text{B}(\text{C}_6\text{H}_5)_4^-$ . The low temperature limit ( $-122^\circ$ )  $^{31}\text{P}\{^1\text{H}\}$  nmr spectrum for a solution of this complex in chlorodifluoromethane is shown in Figure 2 together with a spectrum simulated using an  $\text{A}_2\text{B}_3$  model. The chemical shift of the equatorial phosphorus nuclei is to high field and the chemical shift difference is almost temperature independent. The relatively large chemical shift difference is an additional advantage in establishing intramolecular exchange. As the temperature is raised, two types of line shape effects can be observed (Figure 3): (a) the quadrupole relaxation of the  $^{59}\text{Co}$  nucleus becomes less effective and the upfield side of the spectrum begins to broaden more than the downfield side (again  $J_{\text{PnCo}} > J_{\text{PaCo}}$ ;  $\text{M} = \text{Co}$ , configuration 1); (b) simul-

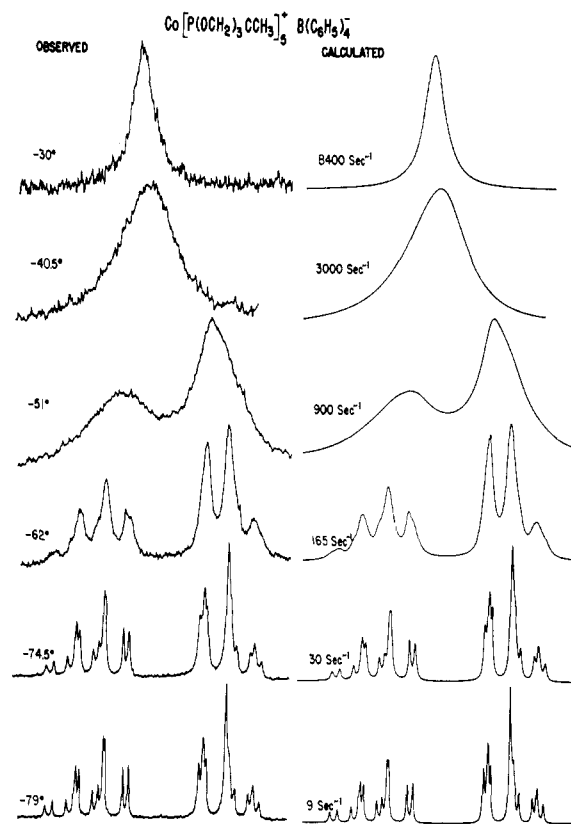


**Figure 3.** Temperature-dependent Fourier mode  $^{31}\text{P}\{^1\text{H}\}$  nmr spectra for a solution of  $\text{Co}[\text{P}(\text{OCH}_2)_3\text{CCH}_3]_5^+ \text{B}(\text{C}_6\text{H}_5)_4^-$  in chlorodifluoromethane. The calculated spectra were obtained using permutational mechanism A.

taneously, line shape effects can be observed that are a result of a mutual exchange process. Figure 3 compares the observed temperature dependence of the nmr spectrum with that simulated using a complete density matrix line shape analysis. In the simulations a permutational mechanism, A, which simultaneously switches the two axial ligands with two of the equatorial ligands was used. This gives a better fit to the observed spectra than the other possible permutational mechanism, B, which involves single axial equatorial switches (see the Discussion section). The spectra in Figure 3 ( $\delta/J = 5.1$ ) are very similar to those observed for  $\text{Ni}[\text{P}(\text{OCH}_2)_3\text{CC}_2\text{H}_5]_5^{2+}(\text{BF}_4)_2$  ( $\delta/J = 4.74$ ); for the latter molecule a detailed comparison has been made between the observed spectra and those simulated for both A and B permutational exchanges (*vide infra*). A comparison of these simulations with the spectra of  $\text{Co}[\text{P}(\text{OCH}_2)_3\text{CCH}_3]_5^+ \text{B}(\text{C}_6\text{H}_5)_4^-$  shown in Figure 3, and with other experimental spectra not shown, clearly indicates that the simultaneous exchange mechanism must predominate for both the  $\text{Ni}^{2+}$  and the  $\text{Co}^+$  complexes. Due to the quadrupolar relaxation effects the fit obtained between the observed and calculated spectra shown in Figure 3 is not as good as for the other  $\text{ML}_5^+$  systems we have analyzed.

The rate data are presented in the form of an Arrhenius plot in Figure 4; the straight line corresponding to the rate expression

$$\text{rate}(T) = 10^{15.28} e^{-12,500/RT}$$

The activation parameters at  $200^\circ\text{K}$  are given in Table II. The apparent entropy of activation is rather large

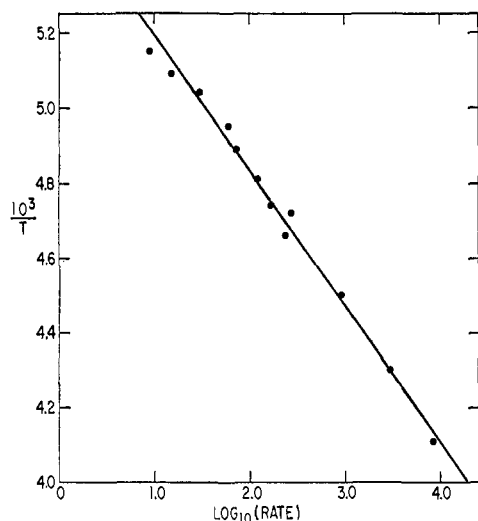


Figure 4. Arrhenius plot for  $\text{Co}[\text{P}(\text{OCH}_2)_3\text{CCH}_3]_5+\text{B}(\text{C}_6\text{H}_5)_4^-$ .

for a simple intramolecular process. This is probably a result of experimental error arising from the limited temperature range over which the measurements were made (the solvent boils at  $-40^\circ$ ) and the errors introduced by the quadrupole relaxation of the  $^{59}\text{Co}$  nucleus.

In a separate experiment the  $^{31}\text{P}\{^1\text{H}\}$  spectra of a solution of  $\text{Co}[\text{P}(\text{OCH}_2)_3\text{CCH}_3]_5+\text{B}(\text{C}_6\text{H}_5)_4^-$  with ligand added were recorded over the temperature range  $-140$  to  $-20^\circ$  in chlorodifluoromethane. The line shapes of the spectrum assigned to the complex were invariant to added ligand, and the ligand resonance remained a sharp single line at all temperatures showing that the exchange process is intramolecular in the  $-140$  to  $-20^\circ$  range.

**C. Iridium.** (i)  $\text{Ir}[\text{P}(\text{OCH}_2)_3]_5+\text{B}(\text{C}_6\text{H}_5)_4^-$ . The temperature-dependent  $^{31}\text{P}\{^1\text{H}\}$  nmr spectrum for a solution of  $\text{Ir}[\text{P}(\text{OCH}_2)_3]_5+\text{B}(\text{C}_6\text{H}_5)_4^-$  in  $\text{CHClF}_2$  is shown in Figure 5. The simulated spectra shown in this figure were obtained using an  $\text{A}_2\text{B}_3$  model assuming mechanism *A*. Since the spectra are almost first order, no distinction can be made in practice between mechanisms *A* and *B*. (This distinction could be made by observing the spectra at a lower field such that higher order effects are present in the slow exchange spectrum.)

The chemical shift difference is quite strongly temperature dependent (approximately  $-5.0 \text{ Hz deg}^{-1}$  or  $-0.15 \text{ ppm deg}^{-1}$  over the temperature range  $-100$  to  $-150^\circ$ ). Consequently an extrapolation of the temperature dependence of the shift difference into the temperature range where the shift cannot be measured directly was used to obtain some of the simulated spectra shown in Figure 5. The large shift difference makes the percentage error introduced by the extrapolation small, and accurate exchange rates can still be obtained even with a rather poor extrapolation. The spectra are invariant to added ligand over the temperature range shown in Figure 5; the ligand resonance remains a sharp single line. This observation is taken to indicate that dissociative processes are slow at these temperatures and that the observed line shape effects can be attributed to an intramolecular process.

From an Arrhenius plot of the data shown in Figure 5 the rate expression

$$\text{rate}(T) = 10^{13.2} e^{-8500/RT} \text{ sec}^{-1}$$

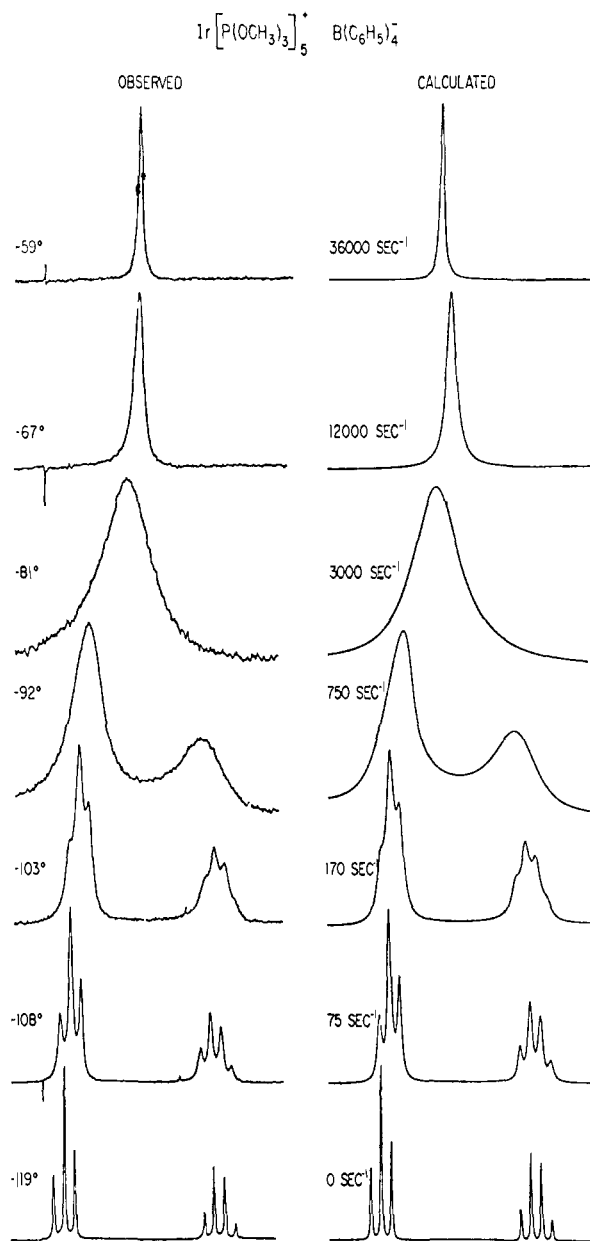


Figure 5. The temperature-dependent Fourier mode  $^{31}\text{P}\{^1\text{H}\}$  nmr spectra for a solution of  $\text{Ir}[\text{P}(\text{OCH}_2)_3]_5+\text{B}(\text{C}_6\text{H}_5)_4^-$  in  $\text{CHClF}_2$  together with spectra simulated using an  $\text{A}_2\text{B}_3$  model and the density matrix formalism.

was obtained. The activation parameters are given in Table II.

(ii)  $\text{Ir}[\text{P}(\text{OC}_2\text{H}_5)_3]_5+\text{B}(\text{C}_6\text{H}_5)_4^-$ . From a complete line shape analysis, we obtained an exchange rate of  $75 \text{ sec}^{-1}$  at  $-60^\circ$ . Substituted into the Eyring equation this result gives a free energy of activation ( $\Delta G^\ddagger$ ) of  $10.4 \text{ kcal mol}^{-1}$ .

(iii)  $\text{Ir}[\text{P}(\text{O}-n\text{-C}_4\text{H}_9)_3]_5+\text{B}(\text{C}_6\text{H}_5)_4^-$ . The exchange rate at  $-42^\circ$  is  $60 \text{ sec}^{-1}$ . This corresponds to a free energy of activation of  $11.5 \text{ kcal mol}^{-1}$  at this temperature.

(iv)  $\text{Ir}[\text{P}(\text{OCH}_2)_3\text{CCH}_3]_5+\text{B}(\text{C}_6\text{H}_5)_4^-$ . The temperature-dependent  $^{31}\text{P}\{^1\text{H}\}$  nmr spectrum for a solution of this complex in chlorodifluoromethane is shown in Figure 6. In this case, the chemical shift difference at low temperatures (slow exchange rates) is essentially temperature independent. In Figure 6 the observed spectra (center of figure) are compared with spectra

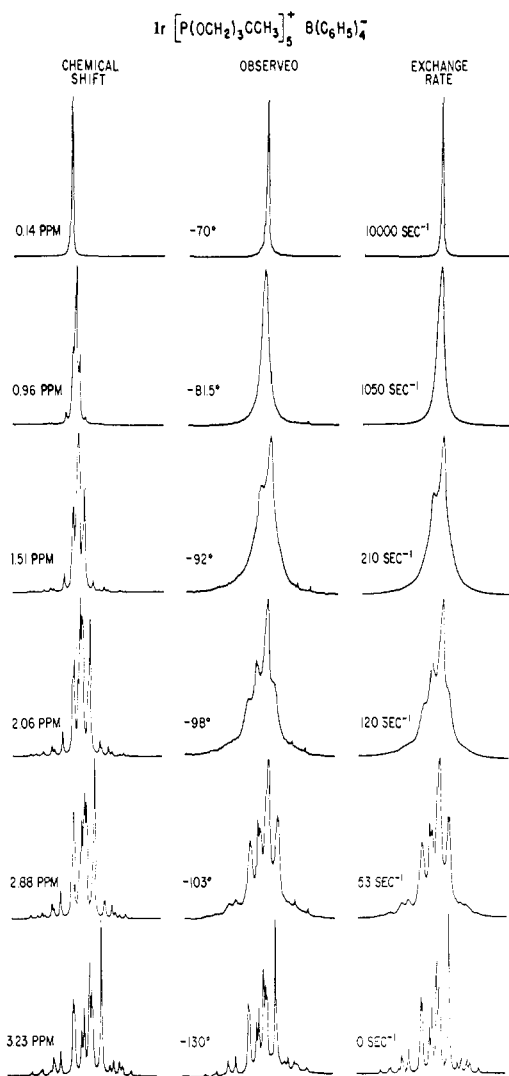


Figure 6. Temperature-dependent Fourier mode  $^{31}\text{P}\{^1\text{H}\}$  nmr spectrum for a solution of  $\text{Ir}[\text{P}(\text{OCH}_2)_3\text{CCH}_3]_5^+\text{B}(\text{C}_6\text{H}_5)_4^-$  in chlorodifluoromethane. The observed spectra are in the middle column. The simulated spectra on the left-hand side were obtained by varying the chemical shift separation only and those on the right-hand side by varying the exchange rate only with the high resolution nmr parameters fixed at their values obtained by fitting the  $-130^\circ$  spectrum.

simulated for a temperature-dependent chemical shift (left-hand side of figure) and for an exchange process in which the two axial ligands are simultaneously exchanged with two of the equatorial ligands (right-hand side of figure). In both sets of simulations the coupling constant was held fixed at 59 Hz. Figure 6 shows that the temperature dependence of the spectra results from an exchange process, rather than from a temperature-dependent shift in the temperature range  $-110$  to  $-60^\circ$ . These results should be compared to those discussed for  $\text{Co}[\text{P}(\text{OC}_2\text{H}_5)_3]_5^+\text{Cl}^-$  (section B (i)) and  $\text{Co}[\text{P}(\text{OCH}_3)_3]_5^+$  (section B (ii)). In all three cases the low temperature limit spectra are quite similar but the temperature dependence of the  $^{31}\text{P}$  spectra for the two Co(I) species can be explained in terms of temperature variations of the chemical shift without invoking exchange, whereas the data for the Ir(I) complex can only be interpreted in terms of chemical exchange.

The rate data obtained from the line shape analysis

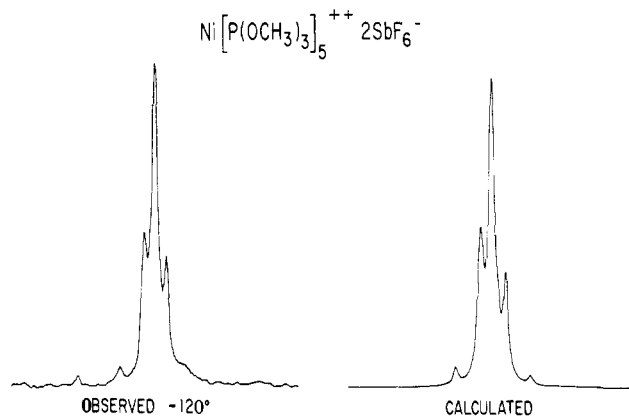


Figure 7. Observed and calculated low temperature limit proton decoupled  $^{31}\text{P}$  nmr spectrum for a solution of  $\text{Ni}[\text{P}(\text{OCH}_3)_3]_5^{2+}(\text{SbF}_6^-)_2$  in chlorodifluoromethane. An  $\text{A}_2\text{B}_3$  model was used to compute the simulated spectrum.

correspond to the Arrhenius expression

$$\text{rate}(T) = 10^{13.5} e^{-9200/RT}$$

The Eyring activation parameters are given in Table II.

**D. Nickel.** (i)  $\text{Ni}[\text{P}(\text{OCH}_3)_3]_5^{2+}(\text{X}^-)_2$ . Figure 7 shows the low temperature limit ( $-120^\circ$ )  $^{31}\text{P}\{^1\text{H}\}$  nmr spectrum for a solution of  $\text{Ni}[\text{P}(\text{OCH}_3)_3]_5^{2+}(\text{SbF}_6^-)_2$  in chlorodifluoromethane together with a spectrum calculated using an  $\text{A}_2\text{B}_3$  model. As the temperature is raised, the spectrum coalesces into a sharp single line. The low temperature limit spectrum is poorly resolved because of the small P-P chemical shift difference. There is no mechanistic information contained in the line shapes and it is not possible to separate the effects of mutual exchange from the effects produced by the temperature dependence of the chemical shift difference.

A number of  $\text{Ni}[\text{P}(\text{OCH}_3)_3]_5^{2+}$  complexes with different anions ( $\text{B}(\text{C}_6\text{H}_5)_4^-$ ,  $\text{PF}_6^-$ ,  $\text{SbF}_6^-$ ,  $\text{AsF}_6^-$ , and  $\text{BF}_4^-$ ) were prepared; their temperature-dependent  $^{31}\text{P}\{^1\text{H}\}$  spectra were invariant to the nature of the anion. These spectra were taken to see whether ion-pairing effects are an important factor in determining the magnitude of the barrier to mutual exchange; these results are inconclusive because of the difficulties encountered in interpreting the temperature dependence although it was demonstrated that the counterion had no effect on the appearance of the low temperature limit spectra (more conclusive anion variation data were presented in a previous paper<sup>2</sup>).

(ii)  $\text{Ni}[\text{P}(\text{OCH}_2)_3\text{CC}_2\text{H}_5]_5^{2+}(\text{BF}_4^-)_2$ . The low temperature limit ( $-125^\circ$ )  $^{31}\text{P}\{^1\text{H}\}$  nmr spectrum of a solution of this complex in chlorodifluoromethane is shown in Figure 8 together with a computer simulation obtained using an  $\text{A}_2\text{B}_3$  model ( $|J_{\text{AB}}| = 119.5$  Hz  $\delta_{\text{A}} - \delta_{\text{B}} = 15.54$  ppm; the axial resonances being to low field).

As the temperature is raised the spectrum at first broadens and then coalesces into a sharp single line. These line shape effects are attributed to an exchange process since the chemical shift separation for the two types of phosphorus is almost temperature independent. The spectra are invariant to added ligand at all temperatures in the range  $-125$  to  $30^\circ$ , and the added ligand resonance remains a sharp single line. Thus, intermolecular exchange processes are not important at these low temperatures.

Figure 9 shows the observed spectrum recorded at

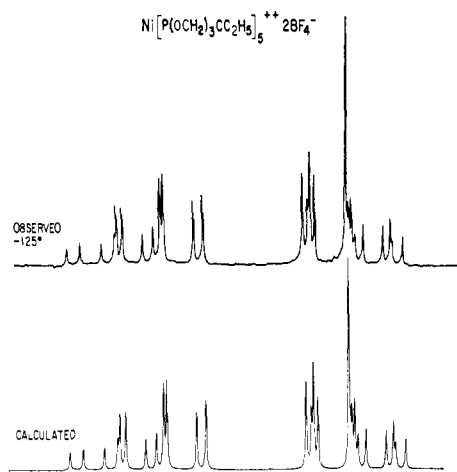


**Figure 8.** Low temperature limit 36.43 MHz Fourier mode  $^{31}\text{P}\{^1\text{H}\}$  nmr spectrum for a solution of  $\text{Ni}[\text{P}(\text{OCH}_2)_3\text{CC}_2\text{H}_5]_5^{2+}(\text{BF}_4^-)_2$  in chlorodifluoromethane. The calculated spectrum was obtained using an  $\text{A}_2\text{B}_3$  model with the parameters given in the text.

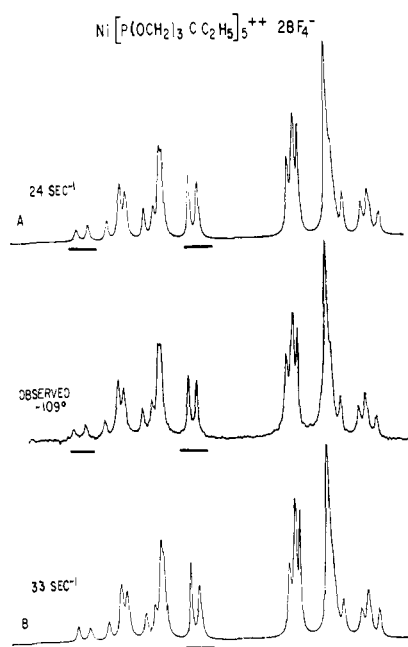


**Figure 9.** A comparison of the observed proton noise decoupled  $^{31}\text{P}$  nmr spectrum of  $\text{Ni}[\text{P}(\text{OCH}_2)_3\text{CC}_2\text{H}_5]_5^{2+}(\text{BF}_4^-)_2$  at  $-109^\circ$  with complete density matrix line shape calculations for the two basic permutational sets *A* and *B*. The two important features which permit a choice to be made in favor of basic set *A* are underlined.

$-109^\circ$  with spectra simulated for the two possible basic permutational sets *A* and *B* for a  $D_{3h}$   $\text{ML}_5$  system (see Discussion section). The two simulated spectra were obtained by varying the exchange rate for each set to give the best visual agreement with the observed spectrum. Both permutational mechanisms give a good fit to the observed spectrum, but it is clear that the fit for set *A* is significantly better. The behavior of the two well-resolved doublets at each end of that part of the spectrum associated mainly with the axial phosphorus nuclei (underlined in Figure 9) is critical in differentiating between *A* and *B*. Figure 10 shows another set of observed and calculated spectra at a somewhat higher temperature (faster exchange rate). The main difference between the two simulated spectra is again found in the two doublets described above and the best

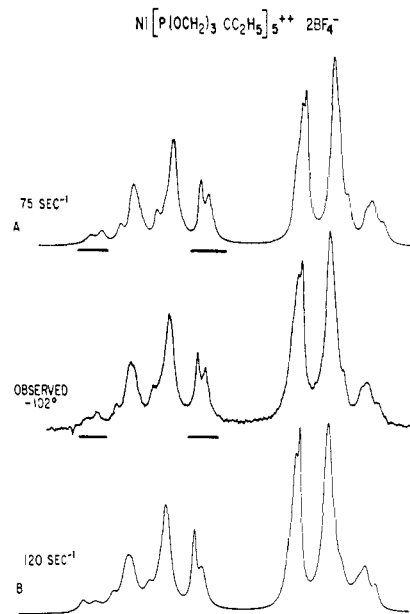


**Figure 10.** A comparison between the observed  $^{31}\text{P}\{^1\text{H}\}$  spectra for  $\text{Ni}[\text{P}(\text{OCH}_2)_3\text{CC}_2\text{H}_5]_5^{2+}(\text{BF}_4^-)_2$  at  $-102^\circ$  and the spectra calculated using basic permutational sets *A* and *B* defined in the text. Again a better fit is given by set *A*. The two important regions of the spectrum which allow this choice to be made are underlined.

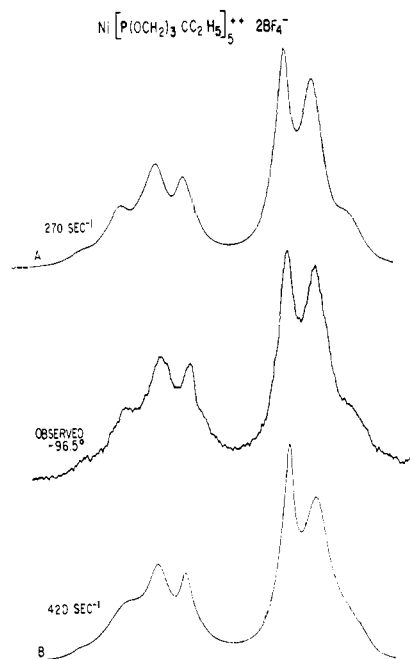


**Figure 11.** This figure compares the observed proton noise decoupled  $^{31}\text{P}$  nmr spectra for a solution of  $\text{Ni}[\text{P}(\text{OCH}_2)_3\text{CC}_2\text{H}_5]_5^{2+}(\text{BF}_4^-)_2$  in chlorodifluoromethane at  $-96.5^\circ$  with spectra simulated using the two basic sets *A* and *B*. Basic set *A* still gives the best fit but in this case the choice does not depend on the features underlined in Figures 9 and 10.

fit is again obtained using basic set *A*. Figure 11 shows a comparison between the observed and simulated spectra at a still higher temperature (exchange rate). Here the distinction between *A* and *B* rests on the behavior of the *high field* part of the spectrum. At higher temperatures (exchange rates) the spectra simulated using basic sets *A* and *B* become more similar, and both give good fits to the observed spectra with set

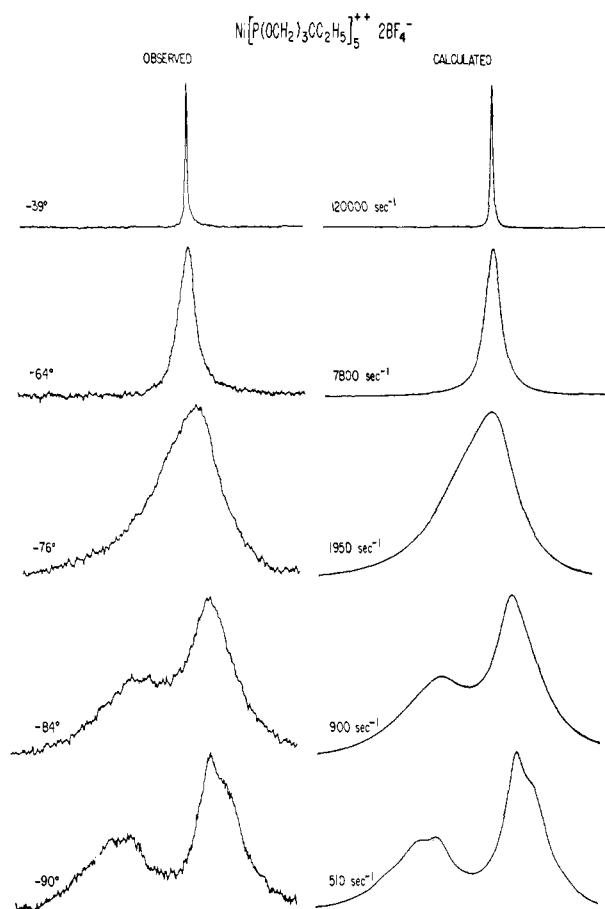


**Figure 12.** Observed and calculated 36.43-MHz Fourier mode proton noise decoupled  $^{31}\text{P}$  nmr spectra for a solution of  $\text{Ni}[\text{P}(\text{OCH}_2)_3\text{CC}_2\text{H}_5]_5^{2+}(\text{BF}_4^-)_2$  in chlorodifluoromethane at temperatures too high for mechanistic information to be obtained. Basic set *A* was used in these simulations.

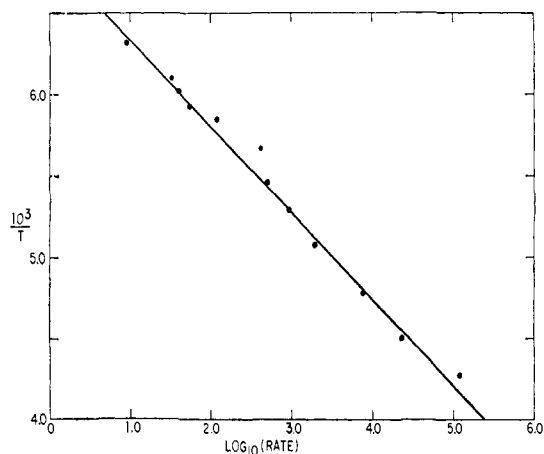


**Figure 13.** Arrhenius plot for  $\text{Ni}[\text{P}(\text{OCH}_2)_3\text{CC}_2\text{H}_5]_5^{2+}(\text{BF}_4^-)_2$  in chlorodifluoromethane.

*B* giving the same result as set *A* at half the exchange rate. Figure 12 compares the observed spectra for  $\text{Ni}[\text{P}(\text{OCH}_2)_3\text{CC}_2\text{H}_5]_5^{2+}(\text{BF}_4^-)_2$  at several temperatures above  $95^\circ$  with those calculated using set *A*.

The rate data are presented in the form of an Arrhenius plot in Figure 13 and may be described by the equation

$$\text{rate}(T) = 10^{12.9} e^{-8600/RT}$$

The activation parameters are given in Table II.

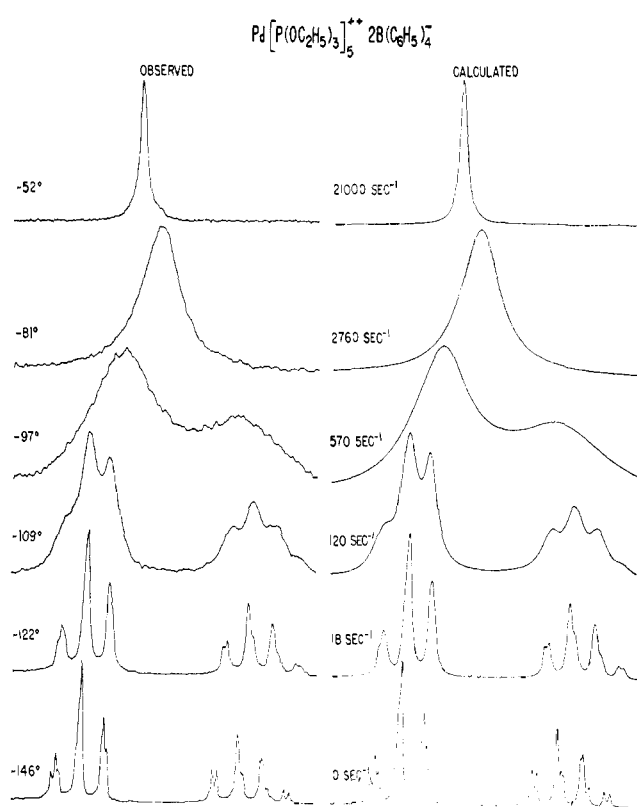


**Figure 14.** Observed and calculated Fourier mode proton decoupled  $^{31}\text{P}$  nmr spectra for a solution of  $\text{Pd}[\text{P}(\text{OC}_2\text{H}_5)_3]_5^{2+}(\text{B}(\text{C}_6\text{H}_5)_4^-)_2$  in chlorodifluoromethane. Permutational mechanism *A* was used in the calculations.

(iii)  $\text{Ni}[\text{P}(\text{OCH}_2)_3\text{CCH}_3]_5^{2+}(\text{BF}_4^-)_2$ . The spectra assigned to this complex are almost identical with those for  $\text{Ni}[\text{P}(\text{OCH}_2)_3\text{CC}_2\text{H}_5]_5^{2+}(\text{BF}_4^-)_2$  at all temperatures in chlorodifluoromethane. The barrier height (free energies of activation) for the exchange process is equal within experimental error to that for the  $\text{P}(\text{OCH}_2)_3\text{CC}_2\text{H}_5$  complex. All observations for  $\text{Ni}[\text{P}(\text{OCH}_2)_3\text{CC}_2\text{H}_5]_5^{2+}(\text{BF}_4^-)_2$  in section D (ii) apply to the methyl cage complex considered here.

(iv)  $\text{Ni}(\text{phosphoradamantane})_5^{2+}(\text{BF}_4^-)_2$ . As in the case for the corresponding  $\text{Rh}(\text{I})$  complex (section A (i)) the temperature dependence of the chemical shift separation is quite small. From a complete density matrix line shape analysis, an exchange rate of  $60 \text{ sec}^{-1}$  at  $-54^\circ$  was obtained giving a free energy of activation of  $10.9 \text{ kcal mol}^{-1}$ .

**E. Palladium.** (i)  $\text{Pd}[\text{P}(\text{OCH}_3)_3]_5^{2+}(\text{B}(\text{C}_6\text{H}_5)_4^-)_2$ . A comparison between the observed spectrum at  $-135^\circ$  and spectra simulated for basic set *A* shows that the exchange rate at this temperature is  $450 \text{ sec}^{-1}$  corresponding to a free energy of activation of  $6.2 \text{ kcal mol}^{-1}$ .

(ii)  $\text{Pd}[\text{P}(\text{OC}_2\text{H}_5)_3]_5^{2+}(\text{B}(\text{C}_6\text{H}_5)_4^-)_2$ . The temperature-dependent  $^{31}\text{P}\{^1\text{H}\}$  nmr spectra for a solution of this complex in chlorodifluoromethane are shown on the left-hand side of Figure 14, calculated spectra (set *A*) are shown on the right. The temperature dependence of the chemical shift difference is relatively small ( $0.012 \text{ ppm deg}^{-1}$  or  $0.45 \text{ Hz deg}^{-1}$  at  $36.43 \text{ MHz}$ ). Basic set *A* gives a slightly better fit than set *B*. The spectra at the lower temperatures in the exchanging region are invariant to added ligand. However, near the fast exchange limit, the spectra broaden on adding ligand indicating that an intermolecular exchange process is

also taking place. Fortunately, the two processes are almost completely separable. The rate data give the Arrhenius expression

$$\text{rate}(T) = 10^{11.9} e^{-7400/RT} \text{ sec}^{-1}$$

The activation parameters are given in Table II.

(iii)  $\text{Pd}[\text{P}(\text{OCH}_2)_3\text{CCH}_3]_5^{2+}(\text{B}(\text{C}_6\text{H}_5)_4^-)_2$ . A comparison between the observed spectrum at  $-146^\circ$  and a density matrix simulation gives an exchange rate of  $480 \text{ sec}^{-1}$  corresponding to a free energy of activation  $\Delta G^\ddagger = 5.7 \text{ kcal mol}^{-1}$ . This is the lowest barrier we have found for an  $\text{ML}_5$  cation.

**F. Platinum.** (i)  $\text{Pt}[\text{P}(\text{OCH}_3)_3]_5^{2+}(\text{B}(\text{C}_6\text{H}_5)_4^-)_2$ . The temperature-dependent  $^{31}\text{P}\{^1\text{H}\}$  nmr spectrum for a solution of this complex in chlorodifluoromethane is shown in Figure 15. Retention of the  $^{31}\text{P}$ - $^{195}\text{Pt}$  coupling in the high temperature limit (Figure 15) demonstrates that the exchange process is intramolecular. A line shape analysis for the  $\text{A}_2\text{B}_3$  pattern corresponding to the 66.3% of molecules with Pt having zero spin gives an exchange rate at  $-130^\circ$  of  $300 \text{ sec}^{-1}$  and a free energy of activation  $\Delta G^\ddagger_{143} = 6.5 \text{ kcal mol}^{-1}$ .

(ii)  $\text{Pt}[\text{P}(\text{OC}_2\text{H}_5)_3]_5^{2+}(\text{B}(\text{C}_6\text{H}_5)_4^-)_2$ . The low temperature limit  $^{31}\text{P}\{^1\text{H}\}$  nmr spectrum for this complex is quite similar to that shown for  $\text{Pt}[\text{P}(\text{OCH}_3)_3]_5^{2+}(\text{B}(\text{C}_6\text{H}_5)_4^-)_2$  in Figure 15. As the temperature is raised the spectrum changes in a similar way to that shown in Figure 15 and the  $^{31}\text{P}$ - $^{195}\text{Pt}$  coupling is retained in the high temperature limit. Calculations give an exchange rate of  $300 \text{ sec}^{-1}$  at  $-74^\circ$  with  $\Delta G^\ddagger_{199} = 9.2 \text{ kcal mol}^{-1}$ .

(iii)  $\text{Pt}[\text{P}(\text{OCH}_2)_3\text{CCH}_3]_5^{2+}(\text{B}(\text{C}_6\text{H}_5)_4^-)_2$ . For this complex and the other Pt and Rh complexes, the analysis of the low temperature limit and of the temperature dependence of the spectra indicate that the couplings of the phosphorus nuclei to the metal nucleus have the same sign for the axial and equatorial phosphorus environments.

Analysis of the line shapes give a rate of  $102 \text{ sec}^{-1}$  at  $-126^\circ$  and a free energy of activation  $\Delta G^\ddagger = 7.0 \text{ kcal mol}^{-1}$ .

## Discussion

**A. The Permutational Analyses.** It has been widely assumed that  $d^8 \text{ML}_5$  species have trigonal bipyramidal stereochemistry ( $D_{3h}$  symmetry) in solution. However, since all previous studies of  $\text{ML}_5$  species in general, and  $d^8$  complexes of group VIII transition metals in particular,<sup>1,12-14</sup> have failed to show inequivalence of nmr ligand resonances even at low temperatures, it was necessary to postulate that the rearrangement barriers were very low ( $<5 \text{ kcal mol}^{-1}$ ). The present studies<sup>1-4</sup> have demonstrated clearly for the first time that a variety of  $\text{ML}_5$  species do indeed have  $D_{3h}$  stereochemistry in solution.

Before discussing the merits of the various possible physical pathways for rearrangement which are consistent with the experimental results for the  $D_{3h}$   $\text{ML}_5$  species described above, we outline what can, and what cannot, be deduced from the permutational analysis and the density matrix calculations.<sup>10</sup>

(12) F. A. Cotton, A. Danti, J. S. Waugh, and R. W. Fessenden, *J. Chem. Phys.*, **29**, 1427 (1958).

(13) R. Bramley, B. M. Figgis, and R. S. Nyholm, *Trans. Faraday Soc.*, **58**, 1893 (1962).

(14) P. Meakin, E. L. Muetterties, and J. P. Jesson, *J. Amer. Chem. Soc.*, **94**, 5271 (1972).

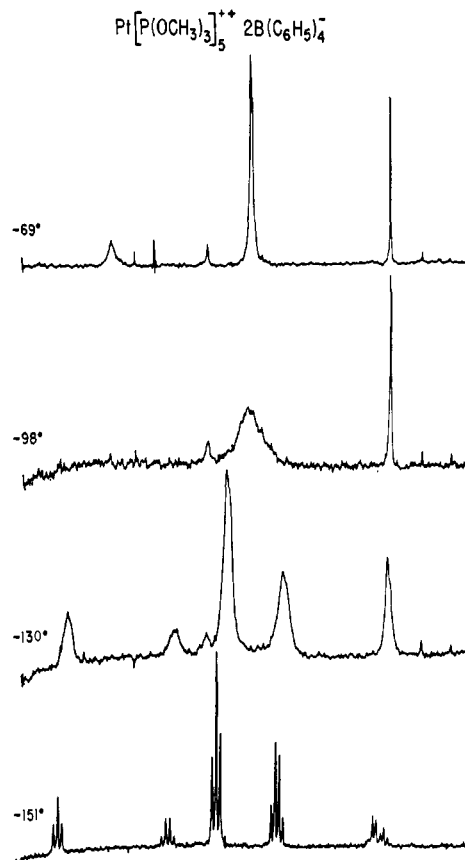
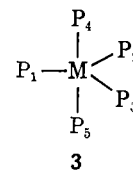


Figure 15. Temperature dependence of the Fourier mode proton decoupled  $^{31}\text{P}$  nmr spectrum assigned to  $\text{Pt}[\text{P}(\text{OCH}_3)_3]_5^{2+}(\text{B}(\text{C}_6\text{H}_5)_4^-)_2$  in chlorodifluoromethane.

The nmr data are analyzed on the basis of a "jump" model and therefore only give information concerning the permutations which relate the initial labeled nuclear configuration to the configuration after rearrangement. No direct mechanistic information is obtained to indicate the actual physical path involved. All routes leading to the correct types of permutational change are equally acceptable, and one must appeal to other chemical information to decide between the possibilities.<sup>10</sup> The possible permutations which convert the initial labeled configuration **3** into all other possible labeled



$D_{3h}$  configurations comprise a group  $P$  of order  $5! = 120$ . These 120 permutations correspond to 120 configurations, many of which are equivalent in the sense that they are related by the operations of the point group of the molecule. Using the numbering in configuration **3** the 12 operations of the  $D_{3h}$  point group may be written as  $g_1 = E = (1)(2)(3)(4)(5)$ ,  $g_2 = C_3^1 = (132)$ ,  $g_3 = C_3^2 = (123)$ ,  $g_4 = C_2(1) = (23)(45)$ ,  $g_5 = C_2(2) = (13)(45)$ ,  $g_6 = C_2(3) = (12)(45)$ ,  $g_7 = \sigma_h = (45)$ ,  $g_8 = S_3^1 = (45)(132)$ ,  $g_9 = S_3^2 = (45)(123)$ ,  $g_{10} = \sigma_v^1(1) = (23)$ ,  $g_{11} = \sigma_v^2(2) = (13)$ , and  $g_{12} = \sigma_v^3(3) = (12)$ .

It can be seen that the 12 operations of  $D_{3h}$  give rise to 12 different permutations using **3** as a basis. Since

the nmr spin Hamiltonian is invariant to the operations of  $G$  ( $G$  is the permutational group generated by the point group of the molecule with elements  $g_i$ ,  $i = 1-12$ ) all of the permutations of  $P$  related by eq 1 for some

$$p_i = g_i p_j g_m \quad (1)$$

$g_i, g_m$  in  $G$  would, if they could occur alone, give the same temperature-dependent nmr line shapes.<sup>10</sup>

At the same time permutations of  $P$  related by eq 2

$$p_i = g_k p_j g_k^{-1} \quad (2)$$

for some  $g_k$  in  $G$  must by symmetry occur at the same rate. We call a set of all of the permutations related by eq 2 a *basic permutational set*.<sup>9,10</sup> Clearly, all members of a basic permutational set must be included together in the line shape calculations for that set; additionally, all such sets comprised of elements related by eq 1 will give the same calculated line shapes and are said to be *equivalent basic permutational sets* (the line shapes will, however, be different from those calculated for any of the individual permutations).<sup>10</sup> Linear combinations of the equivalent basic permutational sets will also give the same calculated line shapes,

In establishing the *basic permutational sets* and *equivalent basic permutational sets* for  $ML_5$  species, we adopt a computational procedure which differs slightly from that described originally for  $H_2ML_4$  molecules with  $C_{2v}$  symmetry.<sup>9</sup> The modifications are necessitated by the fact that  $D_{3h}$ , unlike  $C_{2v}$ , is not an Abelian group and we must therefore take explicit account of the class structure (Abelian groups have only one operation per class). The procedures outlined here will give the correct sets of basic permutations and equivalent permutations for *all groups*, Abelian and non-Abelian alike.

The difference between the two procedures lies in the order in which the conditions eq 1 and 2 are applied. For non-Abelian groups eq 1 must be applied first and the permutations so generated, grouped into basic permutational sets using eq 2; for Abelian groups the order of application is unimportant, as may readily be shown by the following considerations. If we apply eq 2 first, and attempt to generate an equivalent set using eq 1 the following relationship must hold for

$$\sum_{k=1}^{12} g_i g_k p_j g_k^{-1} g_m = \sum_{n=1}^{12} g_n p_q g_n^{-1} \quad (3)$$

some permutation  $p_q$ .

For an Abelian group

$$g_k^{-1} g_m = g_m g_k^{-1} \quad (4)$$

so that we may rewrite eq 3 as

$$\sum_{k=1}^{12} g_k (g_i p_j g_m) g_k^{-1} = \sum_{n=1}^{12} g_n p_q g_n^{-1} \quad (5)$$

noting that  $g_i p_j g_m$  is an element of  $P$  (say  $p_i$ ) establishing that the order of application of eq 1 and 2 in deriving the basic permutational sets is unimportant for Abelian groups. Equation 4 is not true for non-Abelian groups so that, in the present case ( $D_{3h}$ ), we must proceed as follows. Choose a permutation of  $P$  (say  $g_1$ ) and find all the permutations  $e_i$  related to  $g_1$  by eq 1. The set of all  $e_i$  ( $E$ ) clearly consists of the permutations  $g_1-g_{12}$ , the operations of the point group  $G$ . Now select a member of  $E$  (say  $g_1$  again) and find a *basic set* of per-

mutations ( $E(1)$ ) related by eq 2. In this case the basic set contains only one member ( $g_1$ ). Equivalent *basic sets* are generated in the same manner by applying eq 2 to another of the  $e_i$  not yet used (say  $g_2$ ) producing the set  $E(2) = g_2, g_3$  and repeating the process until all the  $e_i$  are exhausted. This gives the following equivalent basic sets  $E(i)$

$$\begin{aligned} E(1) &= g_1 = (1)(2)(3)(4)(5) = E \\ E(2) &= \begin{cases} g_2 = (132) & = C_3^1 \\ g_3 = (123) & = C_3^2 \end{cases} \\ E(3) &= \begin{cases} g_4 = (23)(45) & = C_2(1) \\ g_5 = (13)(45) & = C_2(2) \\ g_6 = (12)(45) & = C_2(3) \end{cases} \\ E(4) &= g_7 = (45) = \sigma_h \\ E(5) &= \begin{cases} g_8 = (45)(132) & = S_3^1 \\ g_9 = (45)(123) & = S_3^2 \end{cases} \\ E(6) &= \begin{cases} g_{10} = (23) & = \sigma_v(1) \\ g_{11} = (13) & = \sigma_v(2) \\ g_{12} = (12) & = \sigma_v(3) \end{cases} \end{aligned}$$

Unlike the Abelian case, the equivalent sets do not contain the same number of permutations; the identity set  $E(1)-E(6)$  is just the group  $D_{3h}$  collected into its classes (as would be expected from the manner of its generation).

We now select another permutation from  $P$  which has not already been used (say (15)(24)) and repeat the procedure described in the previous paragraph generating first a set  $A$  of permutations  $a_i$  satisfying eq 1 (36 permutations) and then the basic sets  $A(j)$  satisfying eq 2. The remaining permutations of  $P$  are exhausted with one more application of the procedure to give the final group of equivalent basic permutational sets  $B(k)$ . Thus we have demonstrated that there are only two possible types of line shape behavior with temperature (other than invariance, basic sets  $E(i)$ ) and these correspond to the basic sets  $A(j)$  and  $B(k)$  ( $j = 1-4$ ;  $k = 1-8$ ). The overall results generated by a computer program are given in Table I. As with the  $E$  sets, the equivalent sets in  $A$  and in  $B$  do not all contain the same number of permutations (the number is 6 or 12 for both  $A$  and  $B$ ). Also the numbers of equivalent sets in  $E$ ,  $A$ , and  $B$  are different (six, four, and eight, respectively).

We may look at Table I from two other points of view. (a) The first is based on the number of distinguishable "isomers" that are possible for a  $D_{3h} ML_5$  molecule in which the nuclei are labeled. This is given by the total number of possible labeled configurations (the 120 configurations generated from a given starting configuration by the 120 permutations in the table) divided by the order of the rotational subgroup of the point group of the molecule (the rotational subgroup of  $D_{3h}$  is  $D_3$  and is of order 6 [ $E + 2C_3 + 3C_2$ ]). We thus obtain the well-known result that there are  $120/6 = 20$  "isomers" or labeled configurations which are not superposable by rotation.

The permutations contained in the identity sets  $E(1)-E(3)$  are all the elements of a permutation group  $R$  generated by the subgroup of proper rotations  $D_3$ ; they therefore generate just one isomer  $I(1)$  from 3. Similarly  $E(4)-E(6)$  contain the permutations corresponding to the remaining operations of the full point

Table I. Basic Permutational Sets and Equivalent Sets for a  $D_{3h}$   $ML_5$  Molecule

	1								
	<i>i</i>	1	2	3	4	5	6		
$E_i(i)$	1	(1)(2)(3)(4)(5)	(132)	(23)(45)	(45)	(45)(132)	(23)		
	2		(123)	(13)(45)		(45)(123)	(13)		
	3			(12)(45)			(12)		
	<i>m</i>								
	<i>j</i>	1	2	3	4				
$A_m(j)$	1	(15)(24)	(1425)	(25)(143)	(15243)				
	2	(14)(25)	(1524)	(14)(253)	(15324)				
	3	(14)(35)	(1534)	(15)(243)	(14325)				
	4	(15)(34)	(1435)	(24)(153)	(14253)				
	5	(25)(34)	(2435)	(15)(234)	(14235)				
	6	(24)(35)	(2534)	(34)(152)	(14352)				
	7			(14)(235)	(15234)				
	8			(35)(142)	(15342)				
	9			(24)(135)	(13425)				
	10			(25)(134)	(13524)				
	11			(35)(124)	(12534)				
	12			(34)(125)	(12435)				
	<i>n</i>								
	<i>k</i>	1	2	3	4	5	6	7	8
$B_n(k)$	1	(25)	(13)(245)	(1325)	(1245)	(13)(25)	(245)	(125)	(13245)
	2	(15)	(23)(145)	(1253)	(2453)	(15)(23)	(145)	(253)	(12453)
	3	(14)	(23)(154)	(1523)	(1452)	(14)(23)	(154)	(152)	(14523)
	4	(35)	(12)(345)	(1532)	(1453)	(12)(35)	(345)	(153)	(14532)
	5	(34)	(12)(354)	(1423)	(1542)	(12)(34)	(354)	(142)	(15423)
	6	(24)	(13)(254)	(1432)	(1543)	(13)(24)	(254)	(143)	(15432)
	7			(1235)	(2345)			(135)	(13452)
	8			(1352)	(1345)			(235)	(12345)
	9			(1342)	(1354)			(234)	(12354)
	10			(1234)	(2354)			(134)	(13542)
	11			(1324)	(1254)			(124)	(13254)
	12			(1243)	(2543)			(243)	(12543)

Chart I

$$p_{sh} = \begin{cases} E_i(i) \equiv \begin{cases} I(1)\{(i = 1; l = 1)(i = 2; l = 1, 2)(i = 3; l = 1-3)\} \\ I(2)\{(i = 4; l = 1)(i = 5; l = 1, 2)(i = 6; l = 1-3)\} \end{cases} \\ A_m(j) \equiv \begin{cases} I(3)\{(j = 1; m = 1, 2)(j = 4; m = 1-4)\} \\ I(4)\{(j = 1; m = 3, 4)(j = 4; m = 5-8)\} \\ I(5)\{(j = 1; m = 5, 6)(j = 4; m = 9-12)\} \\ I(6)\{(j = 2; m = 1, 2)(j = 3; m = 1-4)\} \\ I(7)\{(j = 2; m = 3, 4)(j = 3; m = 5-8)\} \\ I(8)\{(j = 2; m = 5, 6)(j = 3; m = 9-12)\} \end{cases} \\ B_n(k) \equiv \begin{cases} I(9)\{(k = 1; n = 1)(k = 2; n = 1)(k = 3; n = 1, 2)(k = 4; n = 1, 2)\} \\ I(10)\{(k = 1; n = 2)(k = 2; n = 2)(k = 3; n = 3, 4)(k = 4; n = 3, 4)\} \\ I(11)\{(k = 1; n = 3)(k = 2; n = 3)(k = 3; n = 5, 6)(k = 4; n = 5, 6)\} \\ I(12)\{(k = 1; n = 4)(k = 2; n = 4)(k = 3; n = 7, 8)(k = 4; n = 7, 8)\} \\ I(13)\{(k = 1; n = 5)(k = 2; n = 5)(k = 3; n = 9, 10)(k = 4; n = 9, 10)\} \\ I(14)\{(k = 1; n = 6)(k = 2; n = 6)(k = 3; n = 11, 12)(k = 4; n = 11, 12)\} \\ I(15)\{(k = 5; n = 1)(k = 6; n = 1)(k = 7; n = 1, 2)(k = 8; n = 1, 2)\} \\ I(16)\{(k = 5; n = 2)(k = 6; n = 2)(k = 7; n = 3, 4)(k = 8; n = 3, 4)\} \\ I(17)\{(k = 5; n = 3)(k = 6; n = 3)(k = 7; n = 5, 6)(k = 8; n = 5, 6)\} \\ I(18)\{(k = 5; n = 4)(k = 6; n = 4)(k = 7; n = 7, 8)(k = 8; n = 7, 8)\} \\ I(19)\{(k = 5; n = 5)(k = 6; n = 5)(k = 7; n = 9, 10)(k = 8; n = 9, 10)\} \\ I(20)\{(k = 5; n = 6)(k = 6; n = 6)(k = 7; n = 11, 12)(k = 8; n = 11, 12)\} \end{cases} \end{cases}$$

group  $D_{3h}$  and these six permutations generate a second isomer  $I(2)$  from **3**. In general, we may associate six permutations with each isomer; all of the permutations  $p_{h's} = p_{sh}$  ( $s = 1-6$ ), where  $p_h$  is a permutation which generates isomer  $I(h)$  from **3** and  $r_s$  is an element of  $R$ , will generate the same isomer  $I(h)$  from **3**. The overall breakdown in terms of "isomers"  $I(h)$  ( $h = 1-20$ ) (using the notation in Table I) is shown in Chart I. (b) A second way of looking at Table I is based on the number of different nmr spin Hamiltonians for a  $D_{3h}$   $ML_5$  molecule in which the nuclei are labeled. This is given by the total number of permutations in the table (120) divided by the number of permutations which correspond to elements of the effective permutational group of the high resolution nmr Hamiltonian which in this case is isomorphic with the molecular point group  $D_{3h}$ .

These are of course the 12 elements of the identity sets  $E(i)$ . There are therefore  $120/12 = 10$  independent spin Hamiltonians,  $H$  (this is just half the number of "isomers" considered above since the spin Hamiltonian is invariant to  $\sigma_h$  which is not a proper rotation). Each of the ten independent spin Hamiltonians can be generated from the spin Hamiltonian corresponding to **3** by 12 permutations so that we can associate 12 permutations with each spin Hamiltonian. All of the permutations  $p_q g_t$  ( $t = 1-12$ ), where  $p_q$  is a permutation which generates the spin Hamiltonian  $H(q)$  from the spin Hamiltonian for **3** and  $g_t$  is an element of the effective permutational group of the high resolution nmr Hamiltonian, will generate the same spin Hamiltonian  $H(q)$ .

We can then associate 12 of the permutations  $p_i$

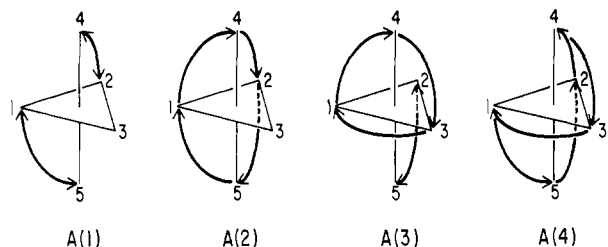


Figure 16. Pictorial representation of the site exchanges effected by the basic permutational sets  $A(j)$ ,  $j = 1-4$ .

(Table I) with each of the ten Hamiltonians by the following relationship

$$p_{iq} = p_{qg_i} \{q = 1-10, t = 1-12\} \quad (6)$$

Using the previous isomer notation for conciseness we have:  $H(1) \equiv I(1), I(2)$ ;  $H(2) \equiv I(3), I(6)$ ;  $H(3) \equiv I(4), I(7)$ ;  $H(4) \equiv I(5), I(8)$ ;  $H(5) \equiv I(9), I(15)$ ;  $H(6) \equiv I(10), I(16)$ ;  $H(7) \equiv I(11), I(17)$ ;  $H(8) \equiv I(12), I(18)$ ;  $H(9) \equiv I(13), I(19)$ ;  $H(10) \equiv I(14), I(20)$ .

This detailed permutational analysis is not necessary to demonstrate that there are only two types of line shape change with temperature ( $A$  or  $B$ ) but it does systematically group all 120 permutations in  $P$  and allow one to select the simplest permutational sets for actually carrying out the line shape calculations. Since there are only ten independent spin Hamiltonians one would expect that basic sets could be chosen such that a total of only ten permutations are involved. Although Table I appears to suggest that a minimum of 13 is required (one for  $E$ , six for  $A$ , and six for  $B$ ) the analysis given above shows that three permutations of the six permutation  $A$  sets are redundant. The simplest set of ten is

$$\begin{aligned} H(1) &= E = (1)(2)(3)(4)(5) \\ \left. \begin{array}{l} H(2) \\ H(3) \\ H(4) \end{array} \right\} &= A = \begin{cases} (15)(24) \\ (14)(35) \\ (25)(34) \end{cases} \\ \left. \begin{array}{l} H(5) \\ H(6) \\ H(7) \\ H(8) \\ H(9) \\ H(10) \end{array} \right\} &= B = \begin{cases} (25) \\ (15) \\ (14) \\ (35) \\ (34) \\ (24) \end{cases} \end{aligned}$$

The line shape analysis establishes that the equivalent sets  $A(1)$ – $A(4)$ , linear combinations of the sets  $A(1)$ – $A(4)$ , or linear combinations of the sets  $A(1)$ – $A(4)$  with  $E(1)$ – $E(6)$  are the ones which give calculated spectra in agreement with experiment. Of the physical processes considered to date<sup>5,6,15</sup> only those corresponding to sets  $A$  or  $B$  alone are likely to have reasonably low barriers. The processes corresponding to  $E$  alone are either proper rotations for the molecule or processes which we would expect to have a high activation energy. The only process which has been considered so far which involves a linear combination of sets ( $A + B + 3E$ )<sup>14</sup> requires a  $D_{5h}$  reaction<sup>15</sup> intermediate. This process would also appear to require a very large activation energy.

Denoting an axial site as "a" and an equatorial site

(15) E. L. Muetterties, *J. Amer. Chem. Soc.*, **91**, 1636, 4115 (1969).

as "e" the sets  $A(1)$ – $A(4)$  may be written as<sup>16</sup>  $A(1) = (ae) \times (ae)$ ,  $A(2) = (aeae)$ ,  $A(3) = (ae) \times (aee)$ , and  $A(4) = (aeae)$  and pictorially as in Figure 16 (the figure represents the overall permutational changes only, it does not imply any particular physical motions effecting the changes).

The detailed line shape analyses described in the first part of the paper have shown for Rh(I), Co(I), Ni(II), and Pd(II) that the permutational nature of the rearrangement is consistent with the  $A(j)$   $\{j = 1-4\}$  (or any linear combination of them with the  $E(i)$   $\{i = 1-6\}$ ) and that mechanisms corresponding to the  $B(k)$  alone are unambiguously ruled out. It seems reasonable to assume that the same permutational behavior applies to all the compounds prepared.

**B. The Rearrangement Barriers.** The free energies of activation for rearrangement in the compounds studied in this paper are collected in Table II together

Table II. Activation Parameters for Intramolecular Rearrangement in  $d^8$   $ML_5$  Cations

Complex	$\Delta G^\ddagger$ , kcal mol <sup>-1</sup>	$\Delta H^\ddagger$ , kcal mol <sup>-1</sup>	$\Delta S^\ddagger$ , cal mol <sup>-1</sup> deg <sup>-1</sup>	Temp, °K
Co <sup>+</sup>				
Temperature dependent shift $\rightarrow 0$ (see text)				
$P(OCH_3)_3$ } $P(OC_2H_5)_3$ } $P(OCH_2)_3CCH_3$	10.0	12.1	10.5	200
Rh <sup>+</sup>				
$P(OCH_3)_3$	7.5	6.3	-6.0	200
$P(OCH_2)_3CCH_3$	7.8			153
$P(OCH_2)_3CC_2H_5$	7.8			150
$P(OC_2H_5)_3$	9.9			208
$P(OCH)_3(CH_2)_3$	10.3			210
$P(O-n-C_4H_9)_3$	11.1			228
Ir <sup>+</sup>				
$P(OCH_3)_3$	8.0	8.1	0.5	200
$P(OCH_2)_3CCH_3$	8.4	8.8	2.0	200
$P(OC_2H_5)_3$	10.4			215
$P(O-n-C_4H_9)_3$	11.5			231
Ni <sup>2+</sup>				
Chemical shift $\sim 0$ (see text)				
$P(OCH_3)_3$ } $P(OC_2H_5)_3$ } $P(OCH_2)_3CCH_3$	$\sim 8.3$	$\sim 8.2$	$\sim -0.5$	200
$P(OCH_2)_3CC_2H_5$	8.3	8.2	-0.5	200
$P(OCH)_3(CH_2)_3$	10.9			220
Pd <sup>2+</sup>				
$P(OCH_2)_3CCH_3$	5.7			127
$P(OCH_3)_3$	6.2			138
$P(OC_2H_5)_3$	8.0	7.0	-5.0	200
Pt <sup>2+</sup>				
$P(OCH_3)_3$	6.5			143
$P(OCH_2)_3CCH_3$	7.0			147
$P(OC_2H_5)_3$	9.2			199

with those for Rh(I) species from an earlier publication.<sup>2</sup> The entropies of activation (with the one exception of  $Co[P(OCH_2)_3CCH_3]_5^+$  where the line shape analysis is complicated by the effects of the <sup>59</sup>Co quadrupolar relaxation and the fact that the temperature range over which accurate rate data can be obtained is relatively small) lie in the range  $-6$  to  $+2$  cal mol<sup>-1</sup> deg<sup>-1</sup>. Small entropies of activation such as these are consistent with a simple intramolecular rearrangement process and the values in Table II are considered to be

(16) J. I. Musher, *J. Amer. Chem. Soc.*, **94**, 5662 (1972).

Table III. Barrier Trends for Varying Central Metals with the Same Ligand

Co[P(OCH <sub>2</sub> ) <sub>3</sub> CCH <sub>3</sub> ] <sub>5</sub> <sup>+</sup>	>	Rh[P(OCH <sub>2</sub> ) <sub>3</sub> CCH <sub>3</sub> ] <sub>5</sub> <sup>+</sup>	<	Ir[P(OCH <sub>2</sub> ) <sub>3</sub> CCH <sub>3</sub> ] <sub>5</sub> <sup>+</sup>
$\Delta G^\ddagger$ , kcal mol <sup>-1</sup> { 10.0		7.8		8.4
∨		∨		∨
8.3	>	5.7	<	7.0
Ni[P(OCH <sub>2</sub> ) <sub>3</sub> CCH <sub>3</sub> ] <sub>5</sub> <sup>2+</sup>		Pd[P(OCH <sub>2</sub> ) <sub>3</sub> CCH <sub>3</sub> ] <sub>5</sub> <sup>2+</sup>		Pt[P(OCH <sub>2</sub> ) <sub>3</sub> CCH <sub>3</sub> ] <sub>5</sub> <sup>2+</sup>

equal within experimental error. The  $\Delta G^\ddagger$  values are accurate to *ca.*  $\pm 0.2$  kcal mol<sup>-1</sup> so that the following meaningful trends can be established from the data.

(i) There is a steady increase in the barrier with increasing steric bulk of the ligand. This is best exemplified by the Rh(I) and Ir(I) series but is consistent also with the data on Pd(II) and Pt(II). The result suggests steric crowding in the transition state relative to the ground state as a principal factor in determining the barrier height. Support for this concept of steric crowding is obtained from the synthetic work<sup>4</sup> which shows that for sufficiently bulky ligands the *D*<sub>3h</sub> ground state can become so unstable that ligand dissociation according to eq 7 occurs to the point where the equilib-



rium is far to the right. Using the ligand cone angle concept<sup>17</sup> as a measure of steric bulk, it appears to be difficult to make *ML*<sub>5</sub> complexes with sizes of the order of P(OC<sub>6</sub>H<sub>5</sub>)<sub>3</sub> (cone angle 128°) or bigger.

(ii) For fixed ligand, the central member of a vertical triad has a lower barrier than the upper or lower members and Co(I) > Ir(I) > Rh(I); Ni(II) > Pt(II) > Pd(II) (see Table III). The data in Table III represent the only complete set, but the trend is supported by other cross comparisons which can be made in Table II and is different from that observed in hydrides of the form HM(PF<sub>3</sub>)<sub>4</sub> where there is a steady increase of barrier on going down a triad.<sup>14</sup>

The trend in barriers down a triad may be tentatively interpreted in terms of a stronger tendency to four *vs.* five coordination for the central member; the lower barrier would then reflect a weaker metal to phosphorus bond either in terms of a lower bending force constant or a longer M–P bond or both; these factors would render the intramolecular rearrangement more facile. This basic picture is supported by preliminary data on intermolecular exchange which suggests that the  $\Delta G_i^\ddagger$  for intramolecular exchange may correlate directly with  $\Delta G_t^\ddagger$  for intermolecular exchange. It is tempting to speculate that for fixed ligand  $\Delta G_t^\ddagger$  is smaller for smaller  $\Delta G_i^\ddagger$  and that for fixed metal  $\Delta G_t^\ddagger$  is smaller for larger  $\Delta G_i^\ddagger$ . The intermolecular exchange studies are not straightforward, and more work is required to definitively establish these suggested trends.

(iii) There is a decrease in barrier on going from a metal of the cobalt triad to the corresponding member of the nickel triad for a given ligand (see Table III). Again, this is opposite to the trend observed for HM-(PF<sub>3</sub>)<sub>4</sub> species on passing from the iron to the cobalt triad (in fact our initial studies of *ML*<sub>5</sub> species were partially directed by the assumption, based on the HM-(PF<sub>3</sub>)<sub>4</sub> results, that increasing positive charge on the central metal would increase the barrier). These results for *ML*<sub>5</sub> species may, however, be rationalized in a similar manner to the results in (ii).

(17) C. A. Tolman, *J. Amer. Chem. Soc.*, **92**, 2956 (1970).

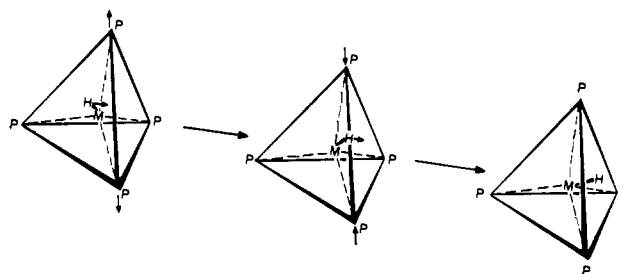


Figure 17. Tetrahedral jump mechanism previously proposed for HML<sub>4</sub> species.<sup>14</sup>

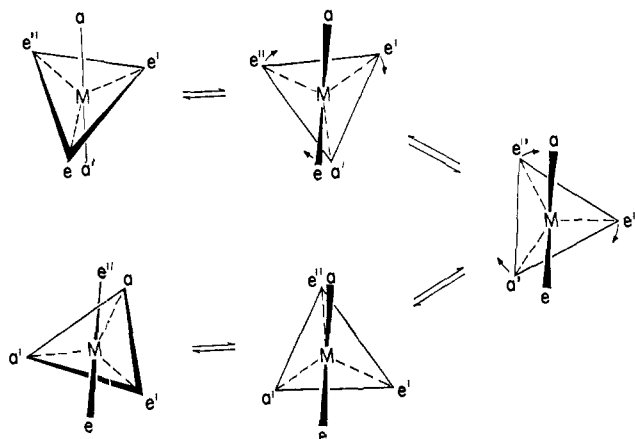
**C. A Comparison between *ML*<sub>5</sub> and HML<sub>4</sub> Rearrangement Barriers.** There are only a few cases where direct comparison can be made (Table IV), but they are

Table IV. Comparison of Barriers for HML<sub>4</sub> and *ML*<sub>5</sub> Compounds

HML <sub>4</sub>	$\Delta G^\ddagger$	<i>ML</i> <sub>5</sub>	$\Delta G^\ddagger$
HFe(PF <sub>3</sub> ) <sub>4</sub> <sup>-</sup>	<5	Fe(PF <sub>3</sub> ) <sub>5</sub>	<5
HRu(PF <sub>3</sub> ) <sub>4</sub> <sup>-</sup>	7	Ru(PF <sub>3</sub> ) <sub>5</sub>	<5
HOs(PF <sub>3</sub> ) <sub>4</sub> <sup>-</sup>	8	Os(PF <sub>3</sub> ) <sub>5</sub>	<5
HCo(PF <sub>3</sub> ) <sub>4</sub>	5.5	Co[P(OC <sub>2</sub> H <sub>5</sub> ) <sub>3</sub> ] <sub>5</sub> <sup>+</sup>	>10
HCo[P(OC <sub>2</sub> H <sub>5</sub> ) <sub>3</sub> ] <sub>4</sub>	<5		
HRh(PF <sub>3</sub> ) <sub>4</sub>	9.0	Rh[P(OC <sub>2</sub> H <sub>5</sub> ) <sub>3</sub> ] <sub>5</sub> <sup>+</sup>	9.9
HRh[P(OC <sub>2</sub> H <sub>5</sub> ) <sub>3</sub> ] <sub>4</sub>	7.3		
HIr(PF <sub>3</sub> ) <sub>4</sub>	10.0	Ir[P(OC <sub>2</sub> H <sub>5</sub> ) <sub>3</sub> ] <sub>5</sub> <sup>+</sup>	10.4
HIr[P(OC <sub>2</sub> H <sub>5</sub> ) <sub>3</sub> ] <sub>4</sub>	?		
HNi[P(OC <sub>2</sub> H <sub>5</sub> ) <sub>3</sub> ] <sub>4</sub> <sup>+</sup>	<5	Ni[P(OC <sub>2</sub> H <sub>5</sub> ) <sub>3</sub> ] <sub>5</sub> <sup>2+</sup>	~10
Fe < Ru < Os		Co > Rh < Ir	
∧ ∧ ∧		∨ ∨ ∨	
Co < Rh < Ir		Ni > Pd < Pt	
Overall electronic control		Overall steric control	

sufficient to allow some tentative conclusions to be drawn. (The limits on the barriers for Co[P(OC<sub>2</sub>H<sub>5</sub>)<sub>3</sub>]<sub>5</sub><sup>+</sup> and Ni[P(OC<sub>2</sub>H<sub>5</sub>)<sub>3</sub>]<sub>5</sub><sup>2+</sup>, which could not be measured directly because of chemical shift separations that were too small or strongly temperature dependent, have been estimated on the basis of the trends in section B.) The barriers for HML<sub>4</sub> species are taken from reference 14.

It can be seen that the barriers for the HML<sub>4</sub> phosphite species are uniformly lower than those for the corresponding *ML*<sub>5</sub> species. However, this may not be true for other ligands and metals which cannot presently be compared. Thus on going from Rh[P(OC<sub>2</sub>H<sub>5</sub>)<sub>3</sub>]<sub>5</sub><sup>+</sup> to Rh[P(OCH<sub>3</sub>)<sub>3</sub>]<sub>5</sub><sup>+</sup> the barrier decreases from 9.9 to 7.5 kcal mol<sup>-1</sup>; if we accept the tetrahedral jump model (Figure 17), which has been proposed for the rearrangement mechanism in HML<sub>4</sub> species,<sup>14</sup> it might be expected that the barrier in HRh[P(OCH<sub>3</sub>)<sub>3</sub>]<sub>4</sub> (not yet measured) would be greater than the value of 7.3 found for HRh[P(OC<sub>2</sub>H<sub>5</sub>)<sub>3</sub>]<sub>4</sub> simply on the grounds that for the latter the smaller size of trimethyl phosphite would lead



**Figure 18.** The turnstile mechanism: the triad ( $e'e'a'$ ) rotates against the ( $ae$ ) pair. The ambiguity in the permutational representation arises in deciding how the initial and final configurations are superposed since they do not superpose in a natural way. Superimposing with  $e'$  in its starting position and  $a$  having been replaced by  $e$ , we get a permutation of the ( $aeae$ ) type. A different superposition choice could lead to an ( $ae$ )  $\times$  ( $ae$ ) type.

to a phosphorus framework which was further from a regular tetrahedron than the phosphorus skeleton of the triethyl phosphite species.

In contrast to the phosphite complexes, those involving trifluorophosphine have barriers that are uniformly lower for the  $ML_5$  complexes than for the  $HML_4$  compounds.

The differing trends and relative barriers from  $ML_5$  to  $HML_4$  cases are almost certainly a reflection of the fact that their ground state geometries are completely different ( $D_{3h}$  in one case and approaching pseudo- $T_d$  in the other) resulting in quite different dependencies of the reaction coordinate from the ground state to the transition state on steric and electronic factors. In fact, if we assume that in the  $HML_4$  series the  $MP_4$  substructure will approach more closely a regular tetrahedron for smaller central metal size (increased ligand–ligand steric interactions), greater formal negative charge on the ligands (increased electrostatic repulsions), and larger steric bulk, these trends will tend to reduce the barrier for the tetrahedral jump.<sup>14</sup> Additionally, since there are only four phosphorus ligands in these molecules the steric factors probably play a secondary role. Thus, a consistent picture can be obtained by postulating that differences in electronic contributions (as opposed to steric) between the ground state and the transition state (Figure 17) are the major factors which determine the barrier for the hydrides. Hence, even though  $PF_3$  is smaller in a steric sense than  $P(OC_2H_5)_3$ , the barrier for  $HRh(PF_3)_4$  is greater than that for  $HRh[P(OC_2H_5)_3]_4$ .

The barrier trends for  $ML_5$  species as noted above lead to exactly the opposite conclusion, namely that steric effects play a dominant role in determining the energy difference between the ground state and the transition state. The suggestion that barriers in the two types of complex are controlled by qualitatively different factors is supported by the considerations in section B (ii) of the discussion.

**D. The Rearrangement Mechanism.** In an earlier paper we discussed briefly the assignment of postulated physical mechanisms to basic permutational sets for five-coordinate trigonal bipyramidal molecules of the form  $MX_5$  ( $D_{3h}$ ),  $MX_4Y$  ( $C_{3v}$ ),  $MX_4Y$  ( $C_{2v}$ ),  $MX_3Y_2$

( $C_{2v}$ ), and  $MX_3Y_2$  ( $C_s$ ). In this section of the discussion we undertake a more detailed examination of the  $MX_5$  case.

Specific physical mechanisms which have been considered in the literature for five-coordinate species are<sup>5,6,15</sup> (i) equatorial–equatorial exchange, (ii) axial–equatorial exchange, (iii) two equatorial–one axial exchange, (iv) two axial–one equatorial exchange, (v)  $D_{3h}$  reaction intermediate, (vi) Berry mechanism, (vii) turnstile mechanism, and (viii) anti-Berry mechanism. This list is somewhat arbitrary and also contains nomenclatures which are primarily permutational in character (e.g., equatorial–equatorial exchange) and others which we associate immediately with particular physical pathways (e.g., Berry process). For the  $ML_5$  species, the first five need not be considered further since they give rise to permutational behavior inconsistent with our experimental results. We now proceed to a more systematic investigation of the problem using the results of section C.

Even if we confine ourselves to overall permutational effects, without inquiring into the actual physical pathway, and omit linear combinations of basic sets, there appear to be 18 possibilities corresponding to the 18 blocks in Table I. (These are in fact reduced to six by the conditions imposed by the possibility of overall rotation of the molecule (*vide infra*.) We could attach names to these possibilities in a similar fashion to those already described in the literature. However, since the results presented in the earlier portion of the paper rule out any physical processes corresponding exclusively to sets  $E(i)$  and  $B(k)$  and since linear combinations are ruled out unless they are almost exclusively  $A$  (mechanism  $v$ , can for instance be ruled out) or combinations of  $A$  and  $E$ , we shall confine our attention to just the sets  $A(j)$  ( $j = 1-4$ ):  $A_1$ , axial–equatorial, axial–equatorial exchange;  $A_2$ , axial–equatorial–axial–equatorial–axial exchange;  $A_3$ , axial–equatorial, axial–equatorial–equatorial–axial exchange;  $A_4$ , equatorial–axial–equatorial–axial–equatorial–equatorial exchange.

The descriptions given above for the sets  $A_1$ – $A_4$  simply state in words the overall permutational effect for each of the sets, no physical mechanism being implied. In assigning a physical mechanism we appeal to other chemical information and, in the absence of evidence to the contrary, choose the mechanism which is the simplest chemically most reasonable process consistent with the facts. This approach is applied to each of the  $A(j)$  below.

( $A(2)$ ,  $A(3)$ ) Care has to be exercised in deciding exactly what we mean when we attempt to associate a given physical mechanism with a particular basic permutational set; in fact we shall show that there are really only two different types of permutational behavior in the  $A(j)$  set, the division into four sets coming simply from additional possibilities of overall rotation of the molecule. Consider for example the turnstile mechanism shown in Figure 18; the drawing is made in such a manner that there is no single well defined way of superimposing the initial and final configurations to write down an unambiguous permutation. Superimposing with  $e'$  in its starting position and  $e$  replacing a gives an ( $aeae$ ),  $A(2)$  type permutation. The reader may readily convince himself that if we impose the restriction that  $e'$  remain in its starting position we always end up with an ( $aeae$ ) type permutation, and, on the other hand, if we

we require  $e'$  not to be in its starting position we always end up with an  $(ae) \times (aee)$ ,  $A(3)$  type permutation. This relationship can also readily be seen from the breakdown into isomers given in section A:  $A(2)$  and  $A(3)$  permutations correspond in pairs to the same isomer.

Similar considerations apply to the Berry mechanism shown in Figure 19. This is perhaps slightly less obvious because of the tendency to talk in terms of the "pivotal" ligand  $e$  which induces one to superimpose the ligand which remains equatorial when in fact this is an arbitrary choice. In fact, the exchange is of the  $(aeae)$   $A(2)$  and  $(ae) \times (aee)$   $A(3)$  type (exactly the same as the turnstile). Attempts to associate  $(aeae)$  with the Berry and  $(ae) \times (aee)$  with the turnstile, although they may be conceptually appealing, are analytically misguided.

$(A(1), A(4))$  From the isomer table we see that these two sets group in the same manner as  $A(2)$  and  $A(3)$  discussed above. A simple  $(ae) \times (ae)$   $A(1)$  pairwise exchange mechanism directly analogous to the permutational representation appears intuitively to be a high energy process as has been pointed out by Musher.<sup>16</sup> However,  $(eaeae)$   $A(4)$  is an equally viable choice and is energetically more appealing in that it could possibly proceed in an overall concerted fashion similar to that shown in Figure 16. The transition state is apparently of low symmetry and difficult to visualize.

As we have seen the  $A(j)$  set gives just two types of behavior. Looking at the isomer table (section A) it can be seen that the  $E(i)$  give just two types as do the  $B(k)$ ; these types have been referred to as *modes* by Musher.<sup>16</sup>

## Conclusion

We have examined the permutational and mechanistic consequences of the spectral data for  $ML_5$  cations in a comprehensive fashion. Clearly, any physical mechanism which corresponds to the mode  $A(2)$ ,  $A(3)$  or to the mode  $A(1)$ ,  $A(4)$  is consistent with the experimental results. However, applying our criteria of additional chemical evidence and conceptual simplicity it appears that the Berry process is by far the most promising candidate for the molecules we are considering.

The Berry mechanism takes specific account of the close relationship of the two most common stereochemistries in five-coordination: the trigonal bipyramid and the square pyramid. A bending mode of a trigonal bipyramidal molecule that involves the two axial and two equatorial bonds leads to a square-pyramidal transition state from which it may return to the original configuration or give a new configuration wherein the permutation of two axial for two equatorial nuclei has been achieved. It is well known that in the solid state square pyramidal forms of five-coordinate species (the transition state in the Berry process) can be established and that geometries intermediate between  $D_{3h}$  and  $C_{4v}$  can also be found. Crystal packing energies are probably comparable to the rearrangement barrier energies we have measured.

The Berry mechanism has been used to interpret a large body of exchange data for five-coordinate molecules and reaction intermediates, and it can, in conjunction with simple stereochemical rules, be used in a predictive sense.

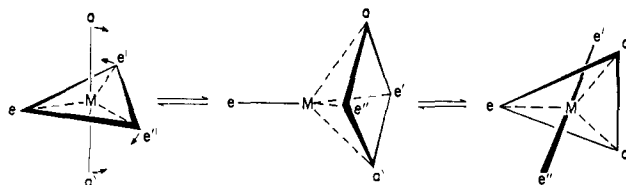


Figure 19. A schematic representation of the Berry mechanism. The two axial ligands exchange positions with two of the equatorial ligands in a single step. The equatorial ligand  $e$  which remains equatorial is called the pivotal ligand. The overall permutation is  $(aeae) = A(2)$ . However,  $(ae) \times (aee)$  is an equally good representation.

We conclude with the simple statement that we believe that, for  $ML_5$  species with  $D_{3h}$  equilibrium stereochemistry, the evidence is strongly in favor of the Berry process as the physical mechanism involved in the rearrangement process and that speculation with regard to alternative mechanisms for this class of compounds is inappropriate in the absence of new experimental or theoretical work which might favor some other physical pathway.

**Acknowledgments.** We would like to thank Mr. M. A. Cushing for preparation of many of the complexes, Messers G. Watunya and J. M. White for obtaining some of the nmr spectra, and Professor John Verkade for kindly supplying a sample of the phosphoradamanthane ligand.

## Appendix

**An Approximation for Nmr Line Shape Analysis.** In a recent paper we discussed two approximations for nmr line shape analysis in complex spin systems.<sup>2</sup> These approximations are (A) omission of lines of low intensity and (B) neglect of the off-diagonal elements of  $(\mathbf{R} + \chi - i\mathbf{L}_o(\omega))$  where  $\mathbf{R}$  is the relaxation matrix,  $\chi$  is the exchange matrix (in Liouville space), and  $\mathbf{L}_o$  is the Liouville operator. In this appendix we consider a third approach in which the matrix  $(\mathbf{R} + \chi - \mathbf{L}_o(\omega))$  is approximately factored. In our calculations this approximate factoring is carried out at the same time as the X factoring and symmetry factoring.<sup>9</sup> In the numerical factoring procedure<sup>9</sup> two transitions  $i$  and  $j$  are considered to be connected by the exchange term  $\chi$  if and only if

$$|\chi_{ij}| > C|\omega_i - \omega_j| \quad (8)$$

where  $\omega_i$  and  $\omega_j$  are the frequencies of the two transitions (in angular frequency units) and  $C$  is a suitably small constant. This factoring procedure is equivalent to setting to zero all of the off-diagonal elements of  $(\mathbf{R} + \chi - \mathbf{L}_o(\omega))$  which do not satisfy condition 8 and rearranging this matrix into block diagonal form ( $\mathbf{M}^-$  is also appropriately rearranged). After the block diagonalization the elements in the diagonal blocks which were set equal to zero because they did not satisfy eq 8 are restored to their original values. If  $C$  is set to a very large value then only degenerate transitions which are connected by  $\chi$  will remain connected after the approximate factoring and this approximation will reduce to approximation B discussed previously (neglect of all off-diagonal elements), except that the degenerate transitions remain connected and spin systems with extensive degeneracies may be treated with confidence at slow exchange rates. However, degenerate transitions may

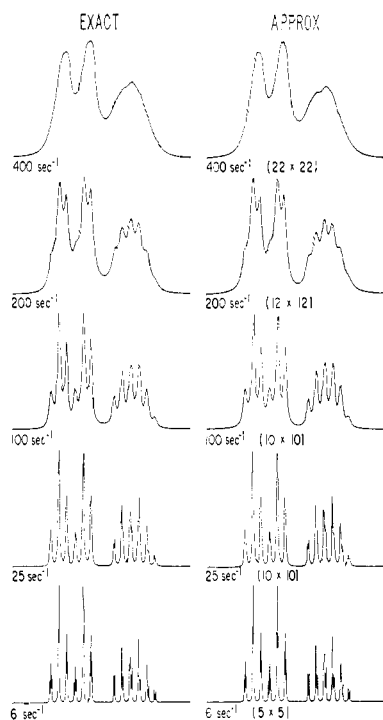


**Figure 20.** Comparison of line shapes calculated using the approximation described in the Appendix with those calculated using a complete calculation. The dimension of the largest complex non-Hermitian matrix which must be diagonalized in the approximate calculations is indicated in parentheses. For the complete calculation this dimension is  $30 \times 30$ .

be treated using approximation B by making an appropriate correction to the diagonal elements of the exchange matrix  $\chi$ . The corrected diagonal elements are given by

$$(\chi_{d_{ii}})_{\text{corr}} = \chi_{d_{ii}} + \left( \sum_j' \chi_{d_{ij}} \mathbf{M}_j^- \right) / \mathbf{M}_i^-$$

In the above equation the subscript  $d$  indicates that the indices vary only over those corresponding to a set of degenerate transitions and the prime on the summation symbol indicates that the term  $\chi_{d_{ii}} \mathbf{M}_i^-$  is excluded. If  $C$  is set to a very small value no approximate factoring is found.

For intermediate values of  $C$  the degree of factoring will depend on the exchange rate(s). At slow rates the approximation will be equal to approximation B (including corrections for degenerate transitions). As the exchange rate is increased, the degree of factoring will decrease until at large exchange rates no approximate factoring will be found, and the complete calculation must be carried out. Figure 20 compares the results of exact and approximate simulation of the nmr line shapes for a trigonal bipyramidal  $A_2B_3X$  system in which the two axial spins ( $A$ ) are simultaneously exchanging with two of the equatorial spins ( $B$ ). In this particular case the constant  $C$  was chosen to have the value  $1/20$ . The slow exchange limit nmr parameters were the same as those used previously ( $J_{AB} = 67.5$  Hz,  $\delta_{AB} = 527$  Hz,  $J_{AX} = 207$  Hz,  $J_{BX} = 142$  Hz). In the present case the approximate calculation using the method outlined above gives better results than approximation B (neglect of all off-diagonal elements). However, the improvement is not dramatic. The utility of this approximation will depend on the nature of the exchange process and the spin system; the example given above probably does not represent a favorable case but was used here for comparison with the two other approximations described previously. Also, it represents a typical  $A_2B_3X$  spin system of the type with which this paper is concerned. The approximation described above and the approximation of neglect of all off-diagonal elements of  $(\mathbf{R} + \chi - i\mathbf{L}_o(\omega))$  may be used in combination with omission of lines of very low intensity to reduce computation time still further.

## Calorimetric and Counterion Binding Studies of the Interactions between Micelles and Ions. The Observation of Lyotropic Series

John W. Larsen\* and Linda J. Magid<sup>1</sup>

Contribution from the Department of Chemistry, University of Tennessee, Knoxville, Tennessee 37916. Received February 14, 1974

**Abstract:** Heats of transfer of a variety of salts from water to solutions of hexadecyltrimethylammonium bromide (CTAB), dodecyltrimethylammonium bromide (DTAB), and sodium dodecyl sulfate (NaLS) were measured. Lyotropic series for both cations and anions were observed for all soaps, the series for the two cationic soaps being almost identical. Linear plots of heats of transfer *vs.* the hydrated radius of the added counterion were observed. Using specific ion electrodes, the competition of tosylate, nitrate, and hydroxide with bromide ion for binding sites on the surface of CTAB micelles was studied. Both tosylate and nitrate bind to the micelle displacing bromide;  $\Delta G$ ,  $\Delta H$ , and  $\Delta S$  for the binding are reported. While addition of hydroxide decreases the amount of bromide bound to the micelle, no binding of hydroxide was observed.

The use of micelles to alter the rates of organic reactions has been vigorously explored by several workers.<sup>2</sup> There are several factors which affect the

size (number of monomers) and shape of micelles and hence their effectiveness in altering organic reaction rates. It is known that addition of salts lower the

(1) NSF Predoctoral Fellow, 1969–1972.  
(2) (a) J. H. Fendler and E. Fendler, *Advan. Phys. Org. Chem.*, **8**, 271 (1970), and references contained therein; (b) "Reaction Kinetics

in Micelles," E. H. Cordes, Ed., Plenum Press, New York, N. Y., 1973, and references contained therein; (c) L. J. Magid, Ph.D. Dissertation, University of Tennessee, 1973.